*Bangladesh Journal of Physics, Vol. **31**, Issue 2, pp. 53 – 65, December 2024*

STUDY OF MOLECULAR TRANSPORT THROUGH NANO-SIZED ASYMMETRIC MULTIPORES IN THE MEMBRANE OF A GIANT UNILAMELLAR VESICLE USING COMSOL SIMULATION

MD. ASADUZZAMAN, SAGOR DAS, SHOVON SAHA, SHAHARIAR EMON, MD. KHORSHED ALAM*

Department of Physics, University of Barishal, Barishal-8254, Bangladesh

**Corresponding author e-mail: dmkalam@bu.ac.bd*

Received on 18.07.2024, Revised received on 26.07.2024, Accepted for publication on 09.08.2024

DOI: *https://doi.org/10.3329/bjphy.v31i2.79519*

ABSTRACT

The controlled transport of molecules through cell membrane nanopores holds significant promise for various biomedical applications, ranging from gene transfection and cancer chemotherapy to transdermal drug delivery. Among the diverse array of membrane-active agents, antimicrobial peptides (AMPs) have garnered substantial interest due to their antibacterial and antifungal properties. Magainin 2, initially uncovered within the African clawed frog *Xenopus laevis*, is one such AMP known to interact with lipid bilayers that lead pore formation induced by membrane-active agents like magainin-2. In this study, we employed simulation techniques using COMSOL Multiphysics to investigate molecular transport of Calcein, Texas-Red Dextran 3000 (TRD-3k), TRD-10k, and AF-SBTI through nanoscale multipores of varying sizes, assessing the impact of both pore diameter and molecular size. Our simulations reveal that the rate constant of molecular transport decreases with increasing fluorescent probe size and pore diameter which comply with experimental observations of inside-to-outside probe leakage.

Keywords: *Nanopores, Molecular transport, Antimicrobial peptides (AMPs), Magainin 2, Giant unilamellar vesicles (GUVs), COMSOL.*

1. INTRODUCTION:

Nanopores embedded within cell membranes serve as gateways for crucial biological processes, offering tantalizing prospects for biomedical advancements. These nanostructures facilitate the controlled passage of molecules, holding promise for targeted therapies and precision medicine applications. Among the diverse array of molecules capable of modulating membrane permeability, antimicrobial peptides (AMPs) stand out for their remarkable antibacterial and antifungal properties, with magainin 2 emerging as a prominent candidate in this regard [1]. Derived from the skin of *Xenopus laevis*, magainin 2 exhibits a remarkable ability to disrupt lipid bilayers and induce the formation of pores [2], [3], [4].

Previous research has extensively explored the behavior of single pores using giant unilamellar vesicles (GUVs). For instance, studies have investigated pore formation induced by various membrane-active agents such as antimicrobial peptides [1], [2], cell-penetrating peptides [5], [6], osmotic pressure [7], nanoparticles [8], [9], mechanical tension [1], [10], [11], and irreversible electroporation [12], [13]. These studies have demonstrated the advantages of using GUVs over smaller vesicles, such as enabling real-time observation of pore formation and fluorescent probe leakage using optical microscopy [5], [13], [14].

Magainin 2-induced pore formation in lipid membranes of vesicles has been particularly well-documented. For example, it was shown that magainin 2 can induce significant leakage of fluorescent probes such as calcein from GUVs, indicating pore formation [1], [15], [16]. These findings are crucial for the development of next-generation drug delivery systems [2], [17]. Furthermore, Tamba and Yamazaki and Tamba et al. described the kinetic pathway of magainin 2-induced pore formation, highlighting the transition from single nanopores to multiple smaller pores [16], [18].

Despite these advancements, the current body of research predominantly focuses on symmetric single-pore systems. For example, studies on the barrel-stave and toroidal pore models [19], [20], [21], [22], [23] have primarily examined single nanopores in symmetric environments. The dynamics of molecular transport through nano-sized asymmetric multipores, particularly within GUV membranes, remain unexplored.

Recent simulation work has shown promise in understanding molecular transport through single nanopores. Jayasooriya and Nawarathna, and Gómez et al. used COMSOL software to simulate molecular transport through a single electroporated nanopore [24], [25]. However, these studies did not address the complexity introduced by asymmetric multipores. The rate constants of molecular transport and pore sizes were derived from single-pore scenarios [16], leaving a significant gap in our understanding of multipore systems.

In this study, we aim to bridge this gap by employing computational simulation techniques to unearth the mechanisms of molecular transport through asymmetric multipores within GUV membranes. Leveraging the computational capabilities of the COMSOL software [26], we model the movement of different fluorescent probes, such as Calcein, Texas-Red Dextran 3000 (TRD-3k), TRD-10k, and AF-SBTI, across nanopores of varying sizes [16]. Our objectives encompass elucidating the influence of both molecular dimensions and pore diameters on the rate of molecular transport, as well as validating our computational model against experimental data [16]. By building upon prior research and incorporating advanced computational techniques, we seek to deepen our understanding of membrane biophysics and advance our knowledge of molecular transport phenomena [18]. Ultimately, this study endeavors to contribute to the development of more efficacious drug delivery systems and precision-targeted therapies, thus driving forward the frontier of biomedical research and innovation.

2. METHODOLOGY:

The simulation was conducted using COMSOL Multiphysics, a software based on the finite element method (FEM) known for its ability to solve complex mathematical problems by segmenting the solution domain into smaller components [27]. This approach allows for the mathematical solution of continuous issues by breaking them down into interconnected challenges. The use of computational tools like COMSOL has become progressively prevalent in recent decades due to their capability to address a wide range of mathematical problems [27]. The simulation setup involved modeling the transport dynamics of molecules through membrane nanopores using the transport of diluted species interface provided by COMSOL. This interface allows for the calculation of the concentration field of a solute species in a solvent, considering mechanisms such as diffusion, convection, and migration. In our study, we focused primarily on diffusion, which governs the passive transport of molecules through the membrane along a concentration gradient.

With COMSOL Multiphysics 5.5, we can simulate the transit of molecules through membrane pores without the need for experiments on living organisms or actual specimens [28]. The

simulation is based on a set of partial differential equations, predefined within COMSOL's transport of diluted species interface, which govern the transport and reactions of dissolved species in a fluid medium. These equations include Fick's second law of diffusion, which describes the rate of change of concentration over time due to diffusion [16]. The simulation setup involved specifying the geometry of the membrane, importing it into COMSOL from AutoCAD (Fig. 1), and defining the materials properties for different regions of the model. Materials properties such as diffusion coefficients and relative permittivity were assigned to simulate the behavior of various components within the system accurately.

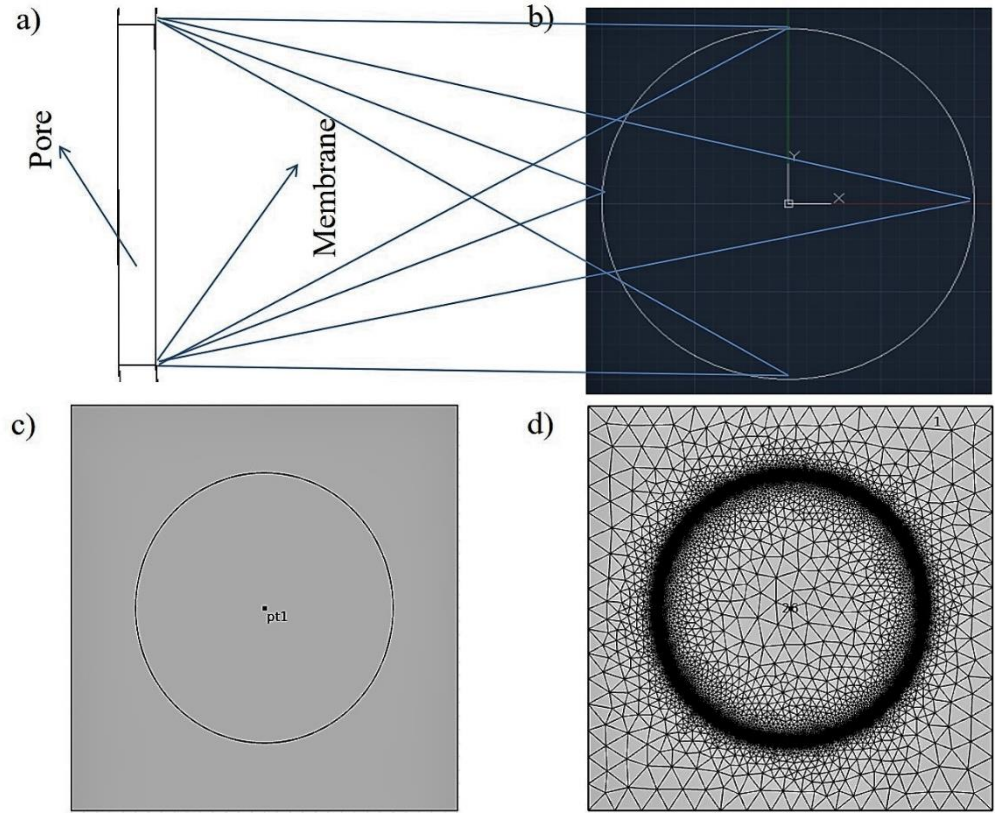

Fig. 1 A GUV with nanopores in its membrane. (a) Closer view of one of nanosized multipores (AutoCAD), scale bar 5 nm. (b) Another view of the multipores (AutoCAD), scale bar 5 μm. (c) 2D membrane geometry (COMSOL simulation). (d) Normal mesh of a GUV (COMSOL).

The simulation techniques employed in our study included designing the membrane geometry in AutoCAD, importing it into COMSOL, and adding materials properties to different regions of the model. This involved creating materials such as buffer solution, cytoplasm, membrane, and aqueous pore, each with specific properties relevant to the simulation.

Additionally, physics interfaces such as the transport of diluted species (tds) were added to the model to simulate the transport of molecules through the membrane nanopores. The transport of diluted species interface allowed for the calculation of concentration fields considering

mechanisms such as diffusion, convection, and migration. Meshing was performed to discretize the geometry model into small, straightforward shape units known as mesh elements. The mesh generator in COMSOL discretizes domains into triangle- or quadrilateral-shaped mesh elements for 2D geometries, allowing for accurate representation of the membrane structure [29].
The study type chosen for our simulation was time-dependent, as it logically suited the diffusion analysis aimed at maximizing the rate of molecular transportation by diffusion. Time-dependent solvers in COMSOL compute solutions over time, providing insights into how the concentration of molecules within the membrane changes over time. The results of the simulation were evaluated and visualized using various tools provided by COMSOL, including data sets, plots, derived values, and export functionalities. Data sets containing concentration values were used to generate plots and plot groups, allowing for the visualization of molecular transport within the membrane nanopores. Additionally, the data obtained from the simulation were exported for further analysis, enabling the fitting of mathematical models to the experimental data [16]. This facilitated a deeper understanding of the diffusion dynamics and provided valuable insights for future studies in membrane biophysics.

3. RESULTS

3.1 Molecular Transport of Various Fluorescent Probes through Asymmetric Multi Nanopores in the Membrane of a GUV

In this subsection, we delve into the molecular transport of fluorescent probes through asymmetric multi nanopores in the membrane of Giant Unilamellar Vesicles (GUVs), focusing on TRD-3k and TRD-10k. Initially, the movement of TRD-3k through asymmetric nanopores into a GUV with a size of 12 μm and suspension area of 130 μm was examined. Fig. 2 (a) illustrates the transit of TRD-3k through a nanopore with a radius of 19 nm into the GUV. At 0 s, the contrast between the interior and exterior of the GUV was represented by red and blue, respectively. COMSOL Multiphysics simulation revealed a progressive rise in the fluorescence intensity of the GUV over time, reaching a steady state at 14.1 s for TRD-3k (Fig. 2 (a, c)).
Comparison with TRD-10k, Calcein, and AF-SBTI indicated variations in fluorescence intensity saturation times [16]. As probe size increased, the time required to reach steady-state fluorescence intensity also increased, demonstrating a size-dependent effect on molecular transport into the GUV (Fig. 2(c)). The saturation time of fluorescence intensity, corresponding to the moment when the outside fluorescence intensity normalized to 1.0, was determined. An analytical treatment based on a single exponential growth function was employed to establish the correlation between the rate constant for molecular transport (k_{mt}) and probe size (R_{SE}).
The time-dependent fluorescence intensities were fitted with the exponential growth function to derive k_{mt} values. For instance, for a 19 nm pore in a 12 μm GUV membrane, the k_{mt} values for TRD-3k and TRD-10k were found to be 0.00444 ± 0.0004 s^{-1} and 0.0027 ± 0.0005 s^{-1}, respectively. Similarly, k_{mt} values were determined for various pore sizes and fluorescent probes, showcasing a decrease in k_{mt} as probe size increased (Fig. 2(f)). The calculated k_{mt} values were consistent with experimental observations, validating the accuracy of the simulation model in representing molecular transport dynamics. Overall, these findings highlight the intricate relationship between nanopore size, fluorescent probe size, and molecular transport kinetics into GUVs, providing valuable insights for future studies in this domain.

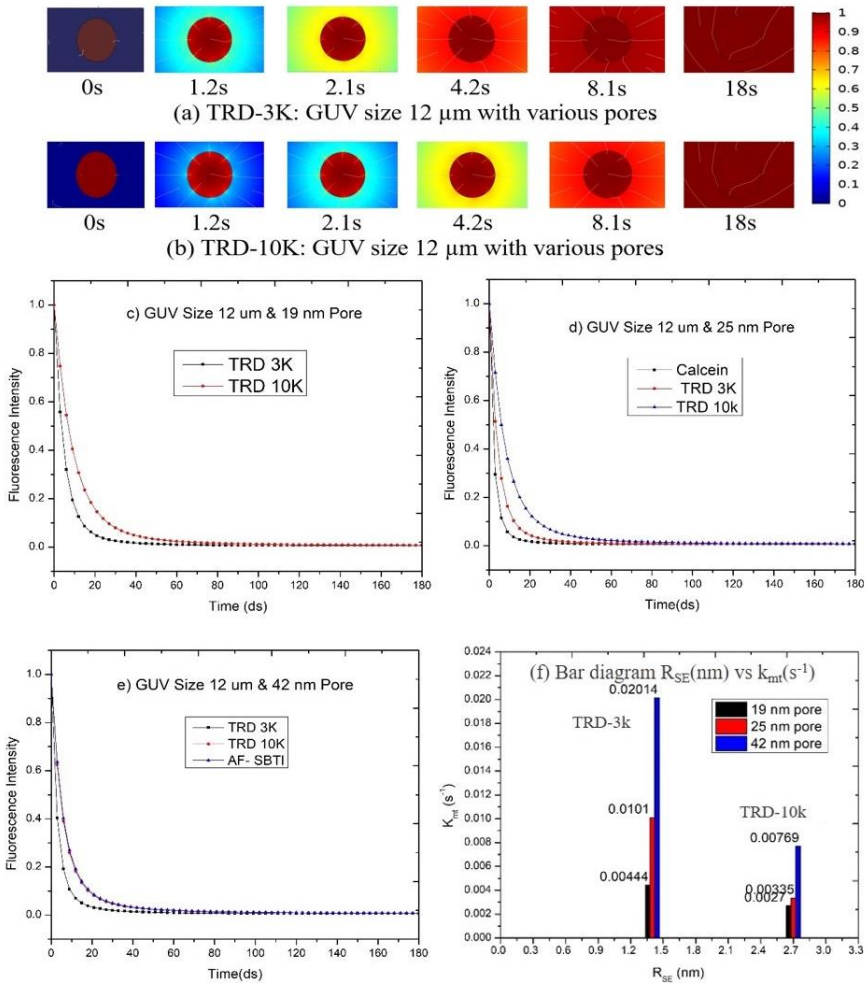

Fig. 2 Molecular concentration changes in GUVs simulated using COMSOL. Panels (a)-(b): Concentration variation over time for TRD3k and TRD10k. Panels (c)-(e): Normalized fluorescence intensity changes for various probes. Panel (f): Rate constant of molecular transport through nanopores of different diameters.

3.2 Comparison of Simulation Findings with Experimental Observations

In this section, we compare the simulation findings of fluorescent probe transport through asymmetric multi nanopores with experimental results reported in previous research [16], focusing on the interaction between magainin 2 and GUVs encasing TRD-3k.

The experimental setup involved the interaction of 7 µM magainin 2 with single GUVs containing TRD-3k. Prior to the addition of magainin 2, phase-contrast microscopy revealed the intact structure of the GUVs, while fluorescence microscopy showed a significant concentration of TRD-3k. Following the addition of magainin 2, a rapid decrease in fluorescence intensity within the GUVs was observed, indicating leakage of TRD-3k through pores generated by magainin 2 within the membrane.

The time-dependent fluorescence intensity demonstrated a sharp decline after approximately 170 s, consistent with the leakage of TRD-3k through membrane pores created by magainin 2. The experimental findings closely aligned with simulation results, where the time required for molecular transport from the interior to the exterior of GUVs was estimated to be between 40 and 100 s for several single GUVs. This timeframe was comparable to the simulation outcomes, which ranged from 20 to 120 s. The similarity between experimental and simulated results validated the accuracy of the simulation model in capturing molecular transport dynamics.

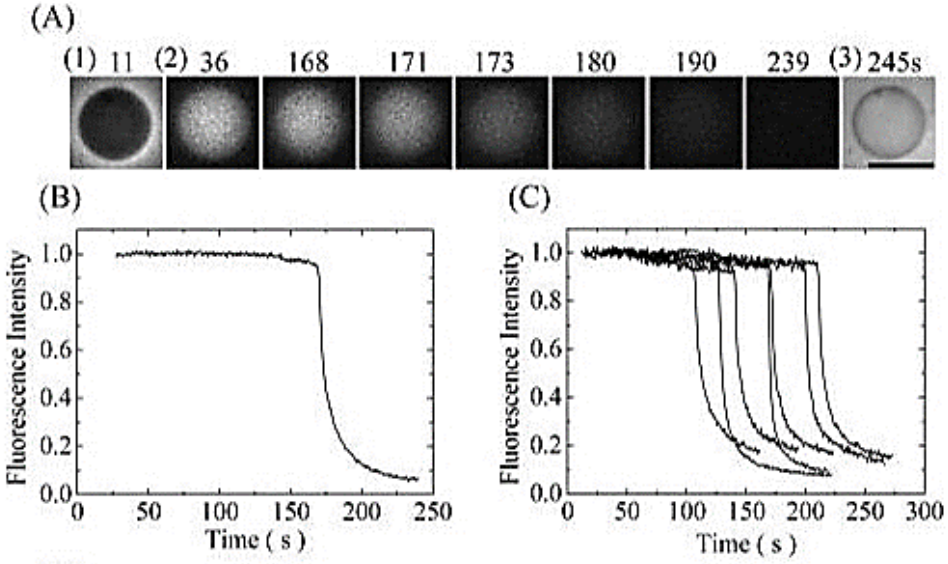

Fig. 3 TRD-3k loss from DOPG/DOPC (5/5) GUV due to 7 μM magainin 2. (a) Fluorescence images show TRD-3k reduction inside a GUV over time. Phase-contrast images at 11 s (1) and 245 s (3) are included. Scale bar: 12 μm. (b) Temporal evolution of GUV fluorescence intensity. (c) Normalized fluorescence intensity variation of multiple GUVs. Reprinted from ref. [16] with permission.

An exponential decay function was applied to fit the reduction in fluorescence intensity observed experimentally, as depicted in Fig. 3. The leakage rate constant (k_{leak}) of fluorescent probes from the interior to the exterior of GUVs through a single pore was determined as 0.0045 ± 0.0004 s^{-1} for an 18 ± 1 nm pore [16]. These k_{leak} values for different fluorescent probes such as Calcein, Texas-Red Dextran 3000 (TRD-3k), TRD-10k, and AF-SBTI, were consistent with the k_{mt} values obtained from the simulation results, as depicted in Fig. 3(f).

Both k_{mt} and k_{leak} represent rate constants, with k_{mt} denoting the rate of molecular transport from the interior to the exterior of GUVs and k_{leak} indicating the rate of fluorescent leakage probes from inside to outside of GUVs through a single pore [16]. The relationship between k_{mt} and k_{leak} is described analytically, emphasizing their similar physical meanings and the consistency observed between experimental and simulated results. The experimental data reported pore sizes ranging from 18 to 46 nm, while the simulation considered pore sizes of 19, 25, and 42 nm, demonstrating comparability between the two datasets. Overall, the agreement between experimental and simulation results underscores the validity of the simulation model in capturing the complex dynamics of molecular transport through nanopores in GUV lipid membranes.

3.3 Investigation of Molecular Transport Through Asymmetric Multi Nanopores Across Various Pore Sizes of a GUV

In this section, we explore the effects of pore diameter on molecular transport through asymmetric multi nanopores in GUV membranes by considering three distinct pore sizes (19, 25, and 42 nm) within a 12 μm GUV. Fig. 3(a–c) illustrates the simulated molecular concentration changes within a GUV for different pore diameters. Before the start of the simulation, the contrast between the inner and outer regions of GUVs remained consistent. The fluorescence intensity within the GUV gradually increased over time as TRD-3k molecules entered through the asymmetric multi nanopores. The time taken for TRD-3k molecules to saturate the GUV varied with pore size, with larger pores reaching saturation faster than smaller ones.

Fig. 3 (d) presents the temporal evolution of fluorescence intensity for pores of various diameters. The fluorescence intensity gradually declines over time before stabilizing at different rates depending on the pore size. This indicates that the size of the GUV's pores influences the rate of molecular transport and saturation of fluorescence intensity within the GUV. Fig. 3(e, f) show the temporal pattern of fluorescence intensity changes for TRD-10k, Calcein, and AF-SBTI in GUVs with different pore sizes. The time required for fluorescence intensity to reach saturation and the rate of fluorescence intensity change varies with probe type and pore size, highlighting the diverse dynamics of molecular transport through nanopores.

Fig. 3(g) displays the time course of k_{mt} for TRD-3k, TRD-10k, Calcein, and AF-SBTI in GUVs with pore sizes of 19, 25, and 42 nm. The mean and standard deviation of k_{mt} values were obtained from five replicate simulations. Consistently, the k_{mt} values decrease as the pore size increases, indicating slower molecular transport through larger pores. The simulation results demonstrate that pore diameter significantly impacts molecular transport dynamics in GUVs. Larger pores facilitate faster molecular transport and saturation of fluorescence intensity within GUVs compared to smaller pores. Furthermore, the type of fluorescent probe also influences the kinetics of molecular transport. Overall, the findings provide valuable understanding of the factors influencing molecular transport through nanopores in GUV membranes.

3.4 Analytical Approach to Molecular Transport Through Nanopores from GUVs

In this section, we delve into the analytical treatment of molecular transport through nanopores from the interior to the exterior of a GUV. We establish the correlation between the rate constant of molecular transport (k_{mt}) and the cross-sectional area of the pore (S_p) through the diffusion of fluorescent probes across the pores. Fick's law governs the flux (J) of a substance per unit area of a pore (S_p), expressed as:

$$J = K \cdot P \cdot [C^{in}(t) - C^{out}(t)] \quad \ldots\ldots\ldots (3.1)$$

where P is the permeability coefficient, C^{in} (t) and C^{out} (t) represent the concentrations of probes inside and outside the GUV at time t, respectively, D_i is the diffusion coefficient, and h is the membrane thickness. The flux (J) can also be expressed as the rate of change of mass (dm/dt) per unit time (t), which leads to:

$$J = \frac{dm}{dt} = \frac{V}{S_p} \cdot \frac{dC^{in}(t)}{dt} \quad \ldots\ldots\ldots\ldots\ldots\ldots (3.2)$$

where V is the volume of the GUV. By combining equations, we arrive at:

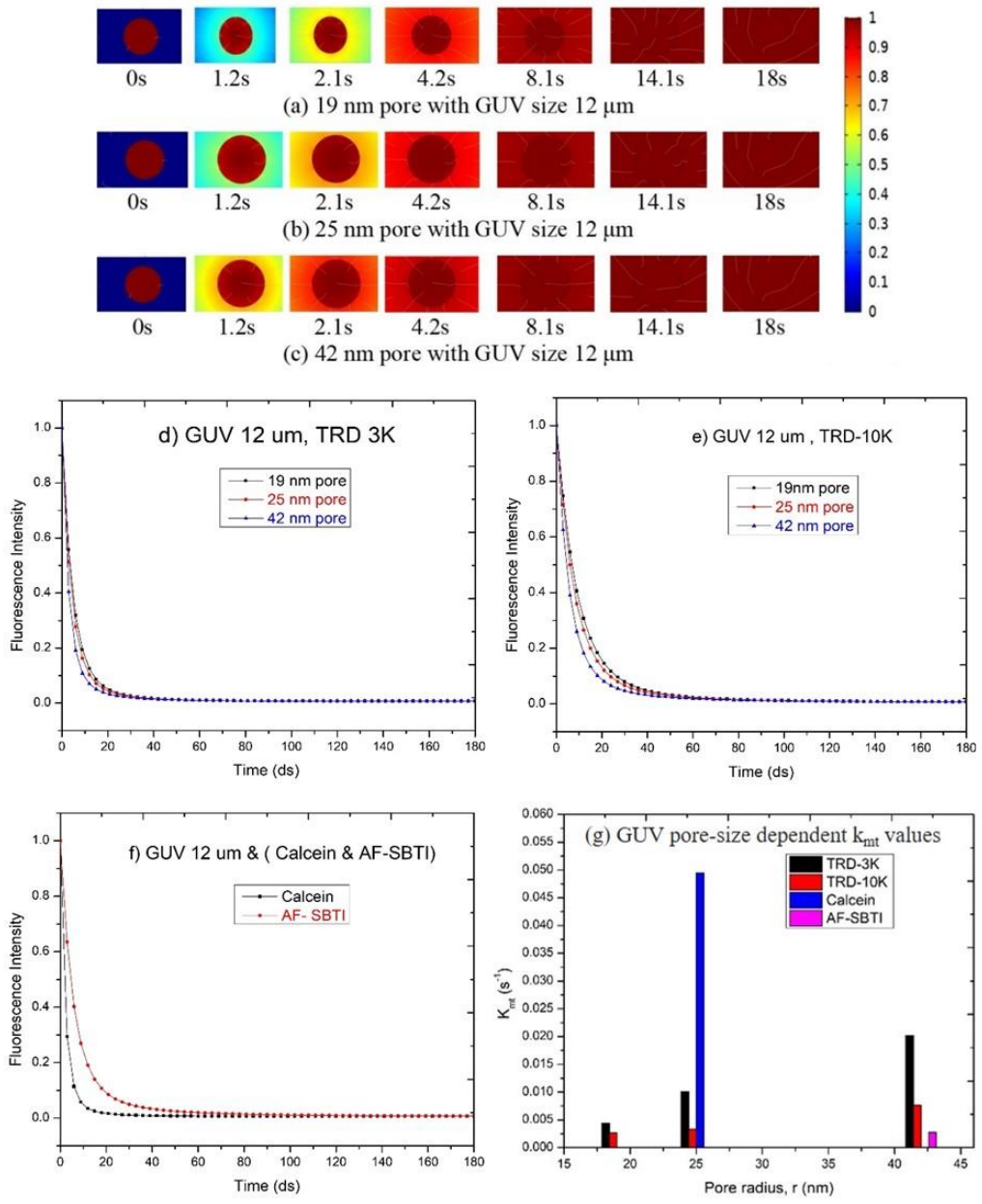

Fig. 3 COMSOL simulations of molecular concentration changes in GUVs across different pore diameters. It includes TRD-3k concentration fluctuations for pore sizes of 19, 25, and 42 nm (a-c), normalized fluorescence intensity changes (d), and variations for TRD-10k and Calcein/AF-SBTI (e-f). Panel (g) illustrates changes in k_{mt} for various fluorescent probes across different pore sizes, providing insights into molecule transport dynamics.

$$\frac{dC_{in}(t)}{dt} = -K \cdot \frac{D_i}{V} \cdot \frac{S_p}{h} \cdot C^{in}(t) \ldots\ldots\ldots\ldots (3.3)$$

The rate of molecular transport of fluorescent probes through the nanopore (k_{mt}) can be expressed as:

$$k_{mt} = K \cdot \frac{0.89 \times 10^{-10} \cdot l}{R_{SE} \cdot d^2} \ldots\ldots\ldots\ldots\ldots\ldots (3.4)$$

where l is the thickness of the membrane, R_{SE} is the effective Stokes radius, and d is the pore diameter. To assess the proposed analytical treatment, we fit the equation to the simulation findings using K as a fitting parameter. Fig. 4 illustrates the dependence of the molecular transport rate constant on the size of the fluorescent probe, with solid lines representing the curve fitting using different values of K. Fig. 5(a) further validates the analytical treatment by depicting the dependence of k_{mt} values on GUV pore diameters for different fluorescent probes. The curve fitting aligns well with the simulation data, indicating a reasonable explanation of the k_{mt} values.

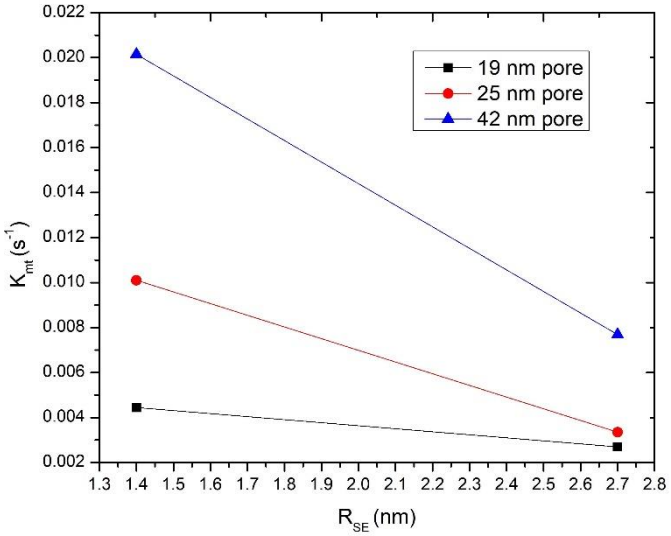

Fig. 4 The molecular transport rate constant through 19, 25, and 42 nm nanopores into the GUV varies with fluorescent probe size. Solid lines (black, red, blue) represent curve fittings with Eq. (3.3) using different K values. Symbols (blue, red) denote k_{mt} values for different probes (R_{SE}) using 25 nm and 42 nm pores, with corresponding curve fittings.

Fig. 5(b) shows the molecular transport rate constant for different fluorescent probes over various nanopores, emphasizing its size dependency. The curve fitting using K as a fitting parameter demonstrates consistency with the simulation results. The analytical treatment presented in this section provides valuable insights into the correlation between pore characteristics and molecular transport dynamics in GUVs. By fitting the analytical model to simulation findings, we validate its effectiveness in explaining the observed phenomena. These insights improve our comprehension of membrane transport processes and pave the way for further exploration in the field.

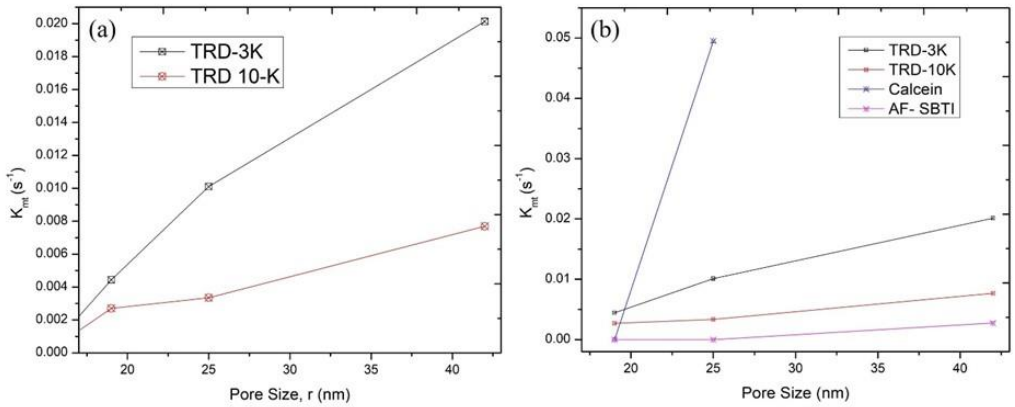

Fig. 5 k_{mt} values for different GUV pore diameters and fluorescent probes. The upper (black) and lower (red) curves in (a) represent TRD-3k and TRD-10k, respectively, fitted with Eq. (3.4) K = 0.00028. In (b), TRD-3k and TRD-10k are in black and red, while Calcein and AF-SBTI are in blue and purple. Solid lines (black and red) show curves fitted with Eq. (3.4) K = 0.00018.

4. DISCUSSION

In this section, we explored the fundamental principles and findings of our study on molecular transport through asymmetric nanopores in Giant Unilamellar Vesicles (GUVs). Passive transport, a process essential for molecular movement across membranes without cellular energy expenditure, served as the focal point of our investigation [30]. Our aim was to elucidate the dynamics of molecular transport from the region of high concentration inside to the region of low concentration outside of GUVs by manipulating the size of fluorescent probes and GUV pore diameters [6].

We employed a fitting approach, utilizing a single exponential decay function, to extract the rate constant (k_{mt}) values for molecular transport. This method, akin to the calculation of cell-penetrating peptide entry rates into GUVs, provided valuable insights into the kinetics of molecular diffusion. Additionally, we applied the Einstein approximation to elucidate the relationship between diffusion time and the diffusion coefficient (D_i) in aqueous solutions. Our simulation results corroborated this relationship, demonstrating that as D_i decreases, the time required for molecular transport increases.

Understanding fluorescent probe diffusion in nanopores necessitates consideration of various frictional effects and interactions within the pore environment. While differences may exist between the probe's diffusion coefficient in the pore and bulk water, our simulation assumed similarity due to the probe's small size relative to the nanopore. We simplified pore structures for computational efficiency, representing them as rectangles with dimensions l and h. The analytical equation (Eq. (3.4)) with the fitting parameter K efficiently captured the molecular transport rate constant, highlighting shared chemical characteristics and interaction patterns among probes.

Comparing simulation results with experimental data, we focused on multiple asymmetric nanopores rather than individual ones. By assuming average pore diameters from experimental data, we identified pore sizes consistent with experimental findings. Our simulation assumed a GUV size of 12 μm, consistent with prior research [1], [2], [6], [10], [14], [30] and employed 2D diffusion as an approximation of 3D diffusion for homogeneous systems.

We maintained consistency in modeling principles across simulation and experimental approaches, including concentration units, Stokes-Einstein equations, Fick's Law, diffusion coefficients, and viscosity. The choice of a 1.0 mol/m³ source concentration for GUV interiors aligned with prior experiments [16], [18], [31], while different probe concentrations were used experimentally to prevent photobleaching without significantly affecting the computation. Despite simplifications for computational efficiency, our simulation effectively captured the influence of pore size on diffusion rate, as evidenced by our results [24]. Overall, our study provides valuable insights into molecular transport through nanopores in GUV membranes, with simulation results complying well with experimental findings. Further research could explore more complex membrane structures and additional factors influencing molecular transport dynamics.

5. CONCLUSION

This study presents a comprehensive investigation into molecular diffusion through asymmetric nanopores within GUV lipid membranes using simulation techniques. Simulation serves as a valuable complement to direct experimental approaches, shedding light on the mechanism of pore creation in vesicle and cell membranes. Our study conducts a thorough investigation into the kinetics of molecular transport across numerous asymmetric nanopore membranes using the GUV cellular model. Simulation results unveil molecular transport through nanopores, with fluorescent probes traversing from the GUV interior to the exterior via asymmetric nanopores. Notably, we observe a decrease in the rate constant of molecular transport with increasing probe size, and conversely, an increase with GUV pore size, consistent with experimental observations. Our research contributes significantly to understanding the molecular aspects of pore creation in biological membranes, with broad implications for biomedical and biotechnological applications. Future endeavors should focus on refining simulation models, considering additional factors such as charge molecule interactions, and integrating multiple physics for enhanced simulation performance. Continued exploration is paramount for advancing our comprehension of molecular transport through peptide-induced nanopores in vesicles, offering valuable insights for diverse applications. We strongly believe simulations study provides an invaluable means to emulate practical experimental settings, facilitating more accurate estimations prior to physical experimentation.

REFERENCES

[1] M. A. S. Karal, J. M. Alam, T. Takahashi, V. Levadny, and M. Yamazaki, “Stretch-activated pore of the antimicrobial peptide, magainin 2,” *Langmuir*, vol. 31, no. 11, pp. 3391–3401, Mar. 2015, doi: 10.1021/la503318z.

[2] M. Hasan, M. A. S. Karal, V. Levadnyy, and M. Yamazaki, “Mechanism of Initial Stage of Pore Formation Induced by Antimicrobial Peptide Magainin 2,” *Langmuir*, vol. 34, no. 10, pp. 3349–3362, Mar. 2018, doi: 10.1021/acs.langmuir.7b04219.

[3] M. A. S. Karal, M. K. Islam, and Z. Bin Mahbub, “Study of molecular transport through a single nanopore in the membrane of a giant unilamellar vesicle using COMSOL simulation,” *European Biophysics Journal*, vol. 49, no. 1, pp. 59–69, Jan. 2020, doi: 10.1007/s00249-019-01412-0.

[4] M. Zasloff, “Magainins, a class of antimicrobial peptides from Xenopus skin: Isolation, characterization of two active forms, and partial cDNA sequence of a precursor (vertebrate peptide antibiotics),” 1987.

[5] M. Z. Islam, H. Ariyama, J. M. Alam, and M. Yamazaki, "Entry of cell-penetrating peptide transportan 10 into a single vesicle by translocating across lipid membrane and its induced pores," *Biochemistry*, vol. 53, no. 2, pp. 386–396, Jan. 2014, doi: 10.1021/bi401406p.

[6] S. Sharmin, M. Z. Islam, M. A. S. Karal, S. U. Alam Shibly, H. Dohra, and M. Yamazaki, "Effects of Lipid Composition on the Entry of Cell-Penetrating Peptide Oligoarginine into Single Vesicles," *Biochemistry*, vol. 55, no. 30, pp. 4154–4165, Aug. 2016, doi: 10.1021/acs.biochem.6b00189.

[7] S. U. Alam Shibly, C. Ghatak, M. A. Sayem Karal, M. Moniruzzaman, and M. Yamazaki, "Experimental Estimation of Membrane Tension Induced by Osmotic Pressure," *Biophys J*, vol. 111, no. 10, pp. 2190–2201, Nov. 2016, doi: 10.1016/j.bpj.2016.09.043.

[8] Y. Roiter, M. Ornatska, A. R. Rammohan, J. Balakrishnan, D. R. Heine, and S. Minko, "Interaction of nanoparticles with lipid membrane," *Nano Lett*, vol. 8, no. 3, pp. 941–944, Mar. 2008, doi: 10.1021/nl0800801.

[9] S. Li and N. Malmstadt, "Deformation and poration of lipid bilayer membranes by cationic nanoparticles," *Soft Matter*, vol. 9, no. 20, pp. 4969–4976, May 2013, doi: 10.1039/c3sm27578g.

[10] M. A. S. Karal and M. Yamazaki, "Communication: Activation energy of tension-induced pore formation in lipid membranes," *Journal of Chemical Physics*, vol. 143, no. 8, Aug. 2015, doi: 10.1063/1.4930108.

[11] M. A. S. Karal, V. Levadnyy, and M. Yamazaki, "Analysis of constant tension-induced rupture of lipid membranes using activation energy," *Physical Chemistry Chemical Physics*, vol. 18, no. 19, pp. 13487–13495, 2016, doi: 10.1039/c6cp01184e.

[12] R. Dimova *et al.*, "Vesicles in electric fields: Some novel aspects of membrane behavior," *Soft Matter*, vol. 5, no. 17. pp. 3201–3212, 2009. doi: 10.1039/b901963d.

[13] M. A. S. Karal, M. K. Ahamed, M. Rahman, M. Ahmed, M. M. Shakil, and K. Siddique-e-Rabbani, "Effects of electrically-induced constant tension on giant unilamellar vesicles using irreversible electroporation," *European Biophysics Journal*, vol. 48, no. 8, pp. 731–741, Dec. 2019, doi: 10.1007/s00249-019-01398-9.

[14] M. A. S. Karal, V. Levadnyy, T. A. Tsuboi, M. Belaya, and M. Yamazaki, "Electrostatic interaction effects on tension-induced pore formation in lipid membranes," *Phys Rev E Stat Nonlin Soft Matter Phys*, vol. 92, no. 1, Jul. 2015, doi: 10.1103/PhysRevE.92.012708.

[15] K. Matsuzaki, O. Murase, N. Fujii, and K. Miyajima, "An Antimicrobial Peptide, Magainin 2, Induced Rapid Flip-Flop of Phospholipids Coupled with Pore Formation and Peptide Translocation †," 1996.

[16] Y. Tamba, H. Ariyama, V. Levadny, and M. Yamazaki, "Kinetic pathway of antimicrobial peptide magainin 2-induced pore formation in lipid membranes," *Journal of Physical Chemistry B*, vol. 114, no. 37, pp. 12018–12026, Sep. 2010, doi: 10.1021/jp104527y.

[17] M. Zasloff, "Antimicrobial peptides of multicellular organisms," 2002. [Online]. Available: www.nature.com

[18] Y. Tamba and M. Yamazaki, "Magainin 2-induced pore formation in the lipid membranes depends on its concentration in the membrane interface," *Journal of Physical Chemistry B*, vol. 113, no. 14, pp. 4846–4852, Apr. 2009, doi: 10.1021/jp8109622.

[19] M. N. Melo, R. Ferre and M. A. R. B. Castanho, "Antimicrobial peptides: linking partition, activity and high membrane-bound concentrations," Nature, vol. 7, pp. 245–250, 2009.

[20] S. J. Ludtke, K. He, W. T. Heller, T. A. Harroun, L. Yang, and H. W. Huang, "Membrane Pores Induced by Magainin †," 1996.

[21] Z. Yang, "Maximum likelihood estimation on large phylogenies and analysis of adaptive evolution in human influenza virus A," *J Mol Evol*, vol. 51, no. 5, pp. 423–432, 2000, doi: 10.1007/s002390010105.

[22] M. T. Lee, F. Y. Chen, and H. W. Huang, "Energetics of Pore Formation Induced by Membrane Active Peptides," *Biochemistry*, vol. 43, no. 12, pp. 3590–3599, Mar. 2004, doi: 10.1021/bi036153r.

[23] X. Qian *et al.*, "In vivo tumor targeting and spectroscopic detection with surface-enhanced Raman nanoparticle tags," *Nat Biotechnol*, vol. 26, no. 1, pp. 83–90, Jan. 2008, doi: 10.1038/nbt1377.

[24] V. Jayasooriya and D. Nawarathna, "Simulation of molecular transport through an electroporated cell using COMSOL Multiphysics," 2017.

[25] O. Henao, V. Gómez, I. De, L. Pava, and J. Sánchez, “Stochastic diffusion of calcium ions through a nanopore in the cell membrane created by electroporation,” 2014.
[26] COMSOL Multiphysics, “https://www.comsol.com/comsol-multiphysics.”
[27] Z. Chen, “Finite element methods and their applications,” p. 410, 2005.
[28] COMSOL Multiphysics, “https://www.comsol.com/comsol-multiphysics/model-builder.”
[29] “COMSOL Documentation.” Accessed: Jul. 15, 2024. [Online]. Available: https://doc.comsol.com/6.2/docserver/#!/com.comsol.help.comsol/helpdesk/helpdesk.html
[30] M. Z. Islam, J. M. Alam, Y. Tamba, M. A. S. Karal, and M. Yamazaki, “The single GUV method for revealing the functions of antimicrobial, pore-forming toxin, and cell-penetrating peptides or proteins,” *Physical Chemistry Chemical Physics*, vol. 16, no. 30. Royal Society of Chemistry, pp. 15752–15767, Aug. 14, 2014. doi: 10.1039/c4cp00717d.
[31] Y. Tamba and M. Yamazaki, “Single giant unilamellar vesicle method reveals effect of antimicrobial peptide magainin 2 on membrane permeability,” *Biochemistry*, vol. 44, no. 48, pp. 15823–15833, Dec. 2005, doi: 10.1021/bi051684w.